Simonenko, S., Bayona, V. y Kindelan, M. (2014). Optimal shape parameter for the solution of elastostatic problems with the RBF method. *Journal of Engineering Mathematics*, 85, pp. 115–129.

DOI: https://doi.org/10.1007/s10665-013-9636-7

J Eng Math (2014) 85:115–129
DOI 10.1007/s10665-013-9636-7

Optimal shape parameter for the solution of elastostatic problems with the RBF method

Stanislav Simonenko · Victor Bayona · Manuel Kindelan

Received: 31 March 2012 / Accepted: 22 February 2013 / Published online: 18 June 2013

Abstract Radial basis functions (RBFs) have become a popular method for the solution of partial differential equations. In this paper we analyze the applicability of both the global and the local versions of the method for elastostatic problems. We use multiquadrics as RBFs and describe how to select an optimal value of the shape parameter to minimize approximation errors. The selection of the optimal shape parameter is based on analytical approximations to the local error using either the same shape parameter at all nodes or a node-dependent shape parameter. We show through several examples using both equispaced and nonequispaced nodes that significant gains in accuracy result from a proper selection of the shape parameter.

Keywords Meshless · Radial basis function (RBF) · RBF–FD · Shape parameter

1 Introduction

The finite-element method (FEM) has become the standard method to numerically solve solid mechanics problems. It is very well suited for problems with irregular geometries that are solved using unstructured grids. However, in recent years considerable efforts have been devoted to *meshless* methods that operate with nodes instead of meshes. Their main advantage is that no mesh generation is required, thereby eliminating one of the most complex steps in the solution procedure. Meshless methods are especially well suited for problems with large deformations, moving discontinuities, or problems that require frequent remeshing.

Radial basis functions (RBFs) are a very successful meshless method that is based on a *global* interpolation using translated RBFs. It was first used as an efficient technique for interpolation of multidimensional scattered data (see [1, Chaps. 1 and 2] and references therein), and later it became popular as a truly mesh-free method for the solution of partial differential equations (PDEs) on irregular domains [2,3]. To overcome some of the drawbacks of this global RBF method, a local RBF method was independently proposed by several authors [4–6]. In this case, the approximation is local, so that it is carried out within a small domain of influence instead of a global one. As a consequence, the resulting linear system is sparse, overcoming the ill-conditioning often associated with the global method, at the cost of losing its spectral accuracy.

S. Simonenko · V. Bayona · M. Kindelan (✉)
Universidad Carlos III, Leganes, Madrid, Spain
e-mail: kinde@ing.uc3m.es

Zhang et al. [7] were the first authors to investigate the capabilities of the global RBF method for the solution of elasticity problems. They considered both globally supported RBFs, such as multiquadrics and thin-plate splines, and compactly supported RBFs, such as Wendland's functions [8]. Later, Tolstykh and Shirobokov [5] applied the local RBF method to the same elasticity problems analyzed in [7] (cantilever beam, plate with a circular hole). Both the global [7] and local [5] approaches are based on the strong formulation of the linear elasticity equations. A third alternative use of RBFs for elasticity problems was proposed by Liu and coworkers [9,10]. It combines the Galerkin weak form and RBFs to form a radial point interpolation method (RPIM). Its performance was analyzed by solving problems involving cantilever beam and a plate with a circular hole.

In recent years, the RBF method has been successfully used to solve a large variety of solid mechanics problems using the global method [11–17], the local method [18–20], or RPIM [21,22]. In most of these works, multiquadrics were used as RBF, and it is well known that accuracy is strongly dependent on the value of the shape parameter. In the case of the local RBF method, we recently proposed an efficient procedure to compute both the optimal constant shape parameter [23] (the same for all nodes) and the optimal variable one [24] (a different shape parameter at each node). The objective of this work is to apply these procedures to elasticity problems and show how the accuracy can be significantly increased by efficiently tuning the values of shape parameters.

The paper is organized as follows: in Sect. 2 we describe the formulation of the global and local RBF method for the solution of plane stress problems. In Sect. 3 we apply these methods to the solution of Timoshenko's beam problem and to the problem of an infinite plate with a circular hole. These problems are solved both with structured and unstructured nodes using either a constant or a variable shape parameter.

2 Formulation

In the case of plane stress problems, the equations of elasticity, written in terms of displacements are,

$$\frac{E}{1-\nu^2}\begin{pmatrix} \dfrac{\partial^2}{\partial x^2}+\dfrac{1-\nu}{2}\dfrac{\partial^2}{\partial y^2} & \dfrac{1+\nu}{2}\dfrac{\partial^2}{\partial x\partial y} \\ \dfrac{1+\nu}{2}\dfrac{\partial^2}{\partial x\partial y} & \dfrac{\partial^2}{\partial y^2}+\dfrac{1-\nu}{2}\dfrac{\partial^2}{\partial x^2} \end{pmatrix}\begin{pmatrix} u \\ v \end{pmatrix}=\begin{pmatrix} f_x \\ f_y \end{pmatrix}. \tag{1}$$

These equations must be solved with appropriate boundary conditions. Once these equations are solved for the displacements, the corresponding stresses can be obtained through

$$\sigma_{xx}=\frac{E}{1-\nu^2}\left(\frac{\partial u}{\partial x}+\nu\frac{\partial v}{\partial y}\right), \tag{2a}$$

$$\sigma_{yy}=\frac{E}{1-\nu^2}\left(\nu\frac{\partial u}{\partial x}+\frac{\partial v}{\partial y}\right), \tag{2b}$$

$$\tau_{xy}=\frac{E}{2(1+\nu)}\left(\frac{\partial u}{\partial y}+\frac{\partial v}{\partial x}\right). \tag{2c}$$

2.1 Global RBF method

In the global RBF method [2,3] we look for an approximate solution in the space spanned by a set of translated RBFs. Thus,

$$u(\mathbf{x})=\sum_{k=1}^{N} a_k\phi_k(r_k(\mathbf{x}),c_u), \tag{3a}$$

$$v(\mathbf{x})=\sum_{k=1}^{N} b_k\phi_k(r_k(\mathbf{x}),c_v), \tag{3b}$$

where $r_k(\mathbf{x}) = ||\mathbf{x} - \mathbf{x}_k||$ is the distance to the RBF center, $||\cdot||$ is the Euclidean norm, $\mathbf{x}_k$ is a set of N RBF centers, and $\phi_k(r_k(\mathbf{x}), c)$ is an RBF function centered at $\mathbf{x}_k$. The unknown coefficients, a_k and b_k, are the coordinates of the approximate solution in the functional space spanned by the RBFs.

A large variety of functions can be used as RBFs. In the rest of the paper we will use Hardy's multiquadric [25],

$$\phi_k(||\mathbf{x} - \mathbf{x}_k||, c) = \sqrt{(x - x_k)^2 + (y - y_k)^2 + c^2}, \tag{4}$$

where c is the shape parameter, which has an important effect in the shape of the RBF. As c increases, the multiquadric becomes flatter, and it is well known that the accuracy of the solution increases exponentially with increasing c until a minimum error is reached for a certain optimal value of c.

The unknown coefficients, a_k, b_k, are computed by collocation of Eq. (1) at a set of interior nodes and collocation of the boundary conditions at boundary nodes. For convenience we will use the same set of RBF centers as collocation nodes. Let us define a vector $\mathbf{z}$ of length $2N$ containing the unknowns

$$\begin{cases} z_k = a_k, \\ z_{k+N} = b_k, \end{cases} \quad k = 1, \ldots, N,$$

and a vector $\mathbf{f}$ containing the forcing terms such that

$$\begin{cases} f_k = f_x(\mathbf{x}_k), \\ f_{k+N} = f_y(\mathbf{x}_k), \end{cases} \quad k = 1, \ldots, N.$$

Substituting Eqs. (3a)–(3b) into Eq. (1) leads to the following linear system:

$$\mathbf{A}\mathbf{z} = \mathbf{f}, \tag{5}$$

where the elements of matrix $\mathbf{A}$ corresponding to an interior node k are, for $i = 1, \ldots, N$,

$$\begin{aligned} A_{k,i} &= \frac{E}{1 - \nu^2}\left[\frac{\partial^2 \phi_k}{\partial x^2}(\mathbf{x}_i) + \frac{1 - \nu}{2}\frac{\partial^2 \phi_k}{\partial y^2}(\mathbf{x}_i)\right], \\ A_{k,i+N} &= \frac{E}{2(1 - \nu)}\frac{\partial^2 \phi_k}{\partial x \partial y}(\mathbf{x}_i), \\ A_{k+N,i} &= \frac{E}{2(1 - \nu)}\frac{\partial^2 \phi_k}{\partial x \partial y}(\mathbf{x}_i), \\ A_{k+N,i+N} &= \frac{E}{1 - \nu^2}\left[\frac{\partial^2 \phi_k}{\partial y^2}(\mathbf{x}_i) + \frac{1 - \nu}{2}\frac{\partial^2 \phi_k}{\partial x^2}(\mathbf{x}_i)\right]. \end{aligned}$$

For boundary collocation nodes the elements of matrix $\mathbf{A}$ depend on the boundary condition. For instance, in the case of Dirichlet boundary conditions,

$$A_{k,i} = \phi_k(||\mathbf{x}_i - \mathbf{x}_k||, c_u), \quad f_k = u_e(\mathbf{x}_k),$$

and

$$A_{k+N,i+N} = \phi_k(||\mathbf{x}_i - \mathbf{x}_k||, c_v), \quad f_{k+N} = v_e(\mathbf{x}_k).$$

Solution of Eq. (5) yields the vector $\mathbf{z}$ and, therefore, the coefficients a_k and b_k of Eqs. (3a) and (3b), which are used to compute the horizontal and vertical displacements u and v, respectively. In addition, the stresses are computed from (2a)–(2c) with

$$\frac{\partial u}{\partial x} = \sum_{k=1}^{N} z_k \frac{\partial \phi_k(||\mathbf{x} - \mathbf{x}_k||, c_u)}{\partial x}, \tag{6a}$$

$$\frac{\partial u}{\partial y} = \sum_{k=1}^{N} z_k \frac{\partial \phi_k(||\mathbf{x} - \mathbf{x}_k||, c_u)}{\partial y}, \tag{6b}$$

$$\frac{\partial v}{\partial x} = \sum_{k=1}^{N} z_{k+N} \frac{\partial \phi_k(||\mathbf{x} - \mathbf{x}_k||, c_v)}{\partial x}, \tag{6c}$$

$$\frac{\partial v}{\partial y} = \sum_{k=1}^{N} z_{k+N} \frac{\partial \phi_k(||\mathbf{x} - \mathbf{x}_k||, c_v)}{\partial y}. \tag{6d}$$

2.2 Local RBF method

In the local RBF method (also known as the RBF finite difference method, RBF–FD) we approximate the differential operator $\mathcal{L}[\cdot]$ at a node $\mathbf{x} = \mathbf{x}_j$ by a linear combination of the values of the unknown function w at n scattered nodes surrounding $\mathbf{x}_j$, which constitute its stencil. Thus,

$$\mathcal{L}[w(\mathbf{x}_j)] \approx \sum_{i=1}^{n} \alpha_{ji} w(\mathbf{x}_i), \tag{7}$$

where α_{ji} are the weighting coefficients. In standard finite differences (FDs), these coefficients are computed using polynomial interpolation. In the RBF–FD formulation, they are computed using interpolation with RBFs. Thus,

$$w(\mathbf{x}) = \sum_{i=1}^{n} \lambda_i \, \phi(r_i(\mathbf{x}), \, c). \tag{8}$$

Substituting (8) into (7) we can determine the unknown weighting coefficients α_{ji} by solving the system of linear equations

$$\mathcal{L}[\phi(r_k(\mathbf{x}_j), c)] = \sum_{i=1}^{n} \alpha_{ji} \phi(r_k(\mathbf{x}_i), \, c), \quad k = 1, \, \ldots, n. \tag{9}$$

Thus, the coefficients α_{ji} depend on the distances from $\mathbf{x}_j$ to the other nodes in the stencil and on the shape parameter c.

Consider, for instance, the second derivative of horizontal displacement with respect to x, u_{xx}, appearing in Eq. (1). With the local RBF method this derivative at x_j is approximated by

$$\frac{\partial^2 u}{\partial x^2}(x_j) \approx \sum_{i=1}^{n} \alpha_{ji} u(x_i), \tag{10}$$

where the coefficients α_{ji} are computed by solving the linear system

$$\mathbf{B}_j \bar{\alpha}_j = \mathbf{q}_j. \tag{11}$$

$\mathbf{B}_j$ is an $n \times n$ matrix whose element in row i column k is given by $\phi_i(r_i(\mathbf{x}_k), c_{uxx})$, and $\mathbf{q}_j$ is a vector whose i component is $\partial^2 \phi_i(r_i(\mathbf{x}_j), c_{uxx})/\partial x^2$. The coefficients to approximate u_{yy}, u_{xy}, v_{xx}, v_{yy}, and v_{xy} are similarly computed. Note that in principle six shape parameters must be chosen (c_{uxx}, c_{uyy}, c_{uxy}, c_{vxx}, c_{vyy}, c_{vxy}).

3 Numerical examples

3.1 Cantilever beam

As a first example we consider a cantilever beam of thickness D, length L, and unit width, which is fully fixed to a support at $x = 0$ and carries an end load P. We use a coordinate system with the y-axis centered at the midplane of the beam. Thus, the upper and lower surfaces of the beam are located at $y = \pm D/2$. The analytic solution of this problem is given by Timoshenko and Goodier [26, Chap. 3] as

$$u_e = -\frac{P}{6EI}\left(y - \frac{D}{2}\right)\left[(6L - 3x)x + (2 + \nu)\left(y^2 - Dy\right)\right], \tag{12a}$$

$$v_e = \frac{P}{6EI}\left[3\nu\left(y - \frac{D}{2}\right)^2 (L - x) + (4 + 5\nu)\frac{D^2 x}{4} + (3L - x)x^2\right], \tag{12b}$$

where E is Young's modulus, ν is Poisson's ratio, and I is the second moment of area of the cross section ($I = D^3/12$ for a narrow rectangular beam of unit width). The stresses corresponding to the preceding displacements are

$$\sigma_{xx} = -\frac{P(L - x)}{I}\left(y - \frac{D}{2}\right), \tag{13a}$$

$$\sigma_{yy} = 0, \tag{13b}$$

$$\tau_{xy} = -\frac{P}{2I}\left(y^2 - Dy\right). \tag{13c}$$

This problem has been widely used to demonstrate the capabilities of adaptive procedures in FEMs, meshless methods, and other numerical techniques. In many cases, however, the boundary conditions necessary to match the exact solution are not used, and therefore conclusions based on errors computed using those solutions are questionable. This fact was recently pointed out by Augarde and Deeks [27]. These authors remark that the displacements given in Eqs. (12a) and (12b) are an exact solution of the plane stress equations only if the load is distributed parabolically [as in Eq. (13c)] and if essential boundary conditions are applied at $x = 0$ according to Eqs. (12a) and (12b).

To be specific, let us consider the displacements of a beam of length $L = 12$, width $D = 2$, Young's modulus $E = 1{,}000$, and Poisson ratio $\nu = 0.3$, to which a vertical force $P = 10$ per unit length is applied at its free end.

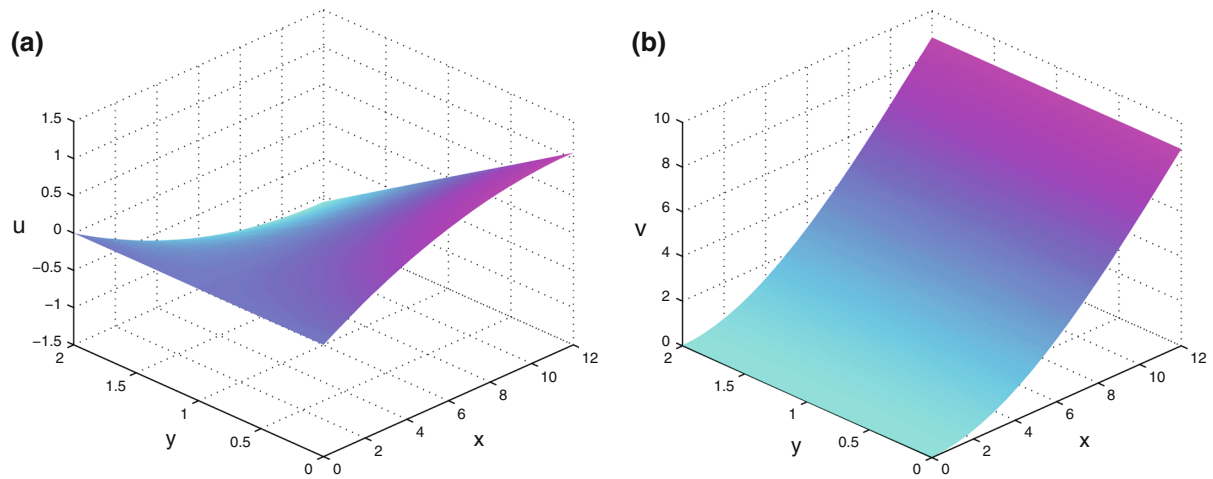

Fig. 1 Exact solution of cantilever beam (12a), (12b) for the case $L = 12,\ D = 2,\ E = 1{,}000,\ \nu = 0.3$. **a** horizontal displacement u. **b** Vertical displacement v

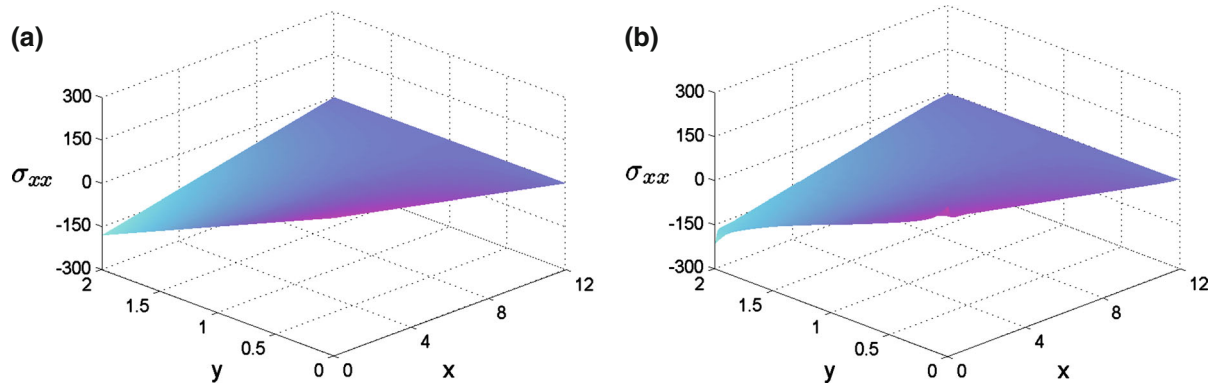

Fig. 2 x stress in the case $L = 12,\ D = 2,\ E = 1{,}000,\ \nu = 0.3$. **a** σ_{xx} (13a) distribution for exact solution. **b** σ_{xx} distribution for boundary conditions $u = v = 0$ at $x = 0$ and $P' = 5$ per unit length at $x = L$

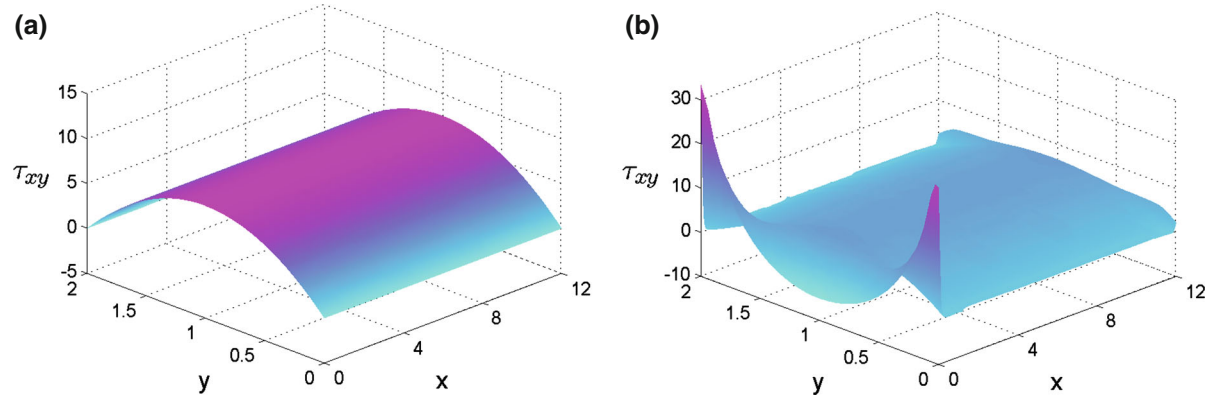

Fig. 3 Shear stress in the case $L = 12,\ D = 2,\ E = 1{,}000,\ \nu = 0.3$. **a** τ_{xy} (13c) distribution for exact solution. **b** Shear stress τ_{xy} distribution for boundary conditions $u = v = 0$ at $x = 0$ and $P' = 5$ per unit length at $x = L$

The solution given by Eqs. (12a) and (12b) is shown in Fig. 1. According to [27], this is the exact solution of the problem with free boundary conditions at $y = 0$ and $y = D$, Dirichlet boundary conditions at $x = 0$ given by (12a)–(12b), and parabolic load at $y = L$:

$$P' = -\frac{6P}{D^3}(y^2 - Dy), \quad \int_0^D P' \mathrm{d}y = P.$$

However, the Timoshenko beam problem is often solved with other boundary conditions. For instance, a common boundary condition used is full fixity at the support and uniform load P at the vertical surface at $x = L$. The solution in terms of displacements with these boundary conditions is very similar to the solution shown in Fig. 1. However, the solution in terms of stresses is quite different, as can be observed in Figs. 2 and 3. These results were obtained using FEMs with a mesh of 6,985 nodes and 13,568 triangular elements. Figure 2 compares the distribution of σ_{xx} of the exact solution (13c) (left part) with the corresponding distribution of σ_{xx} for the problem with fully fixed boundary conditions at $x = 0$ ($u = v = 0$) and uniform load $P' = 5$ per unit length at $x = L$ (right part). Notice that both solutions are quite similar except near $x = 0$, where they differ significantly due to stress concentrations near the borders.

The results for shear stress in Fig. 3 show even greater differences. Notice that the shear stress distribution exhibits singularities at the top and bottom corners that lead to significant differences with the Timoshenko beam solution [Eqs. (13a)–(13c)] throughout the beam.

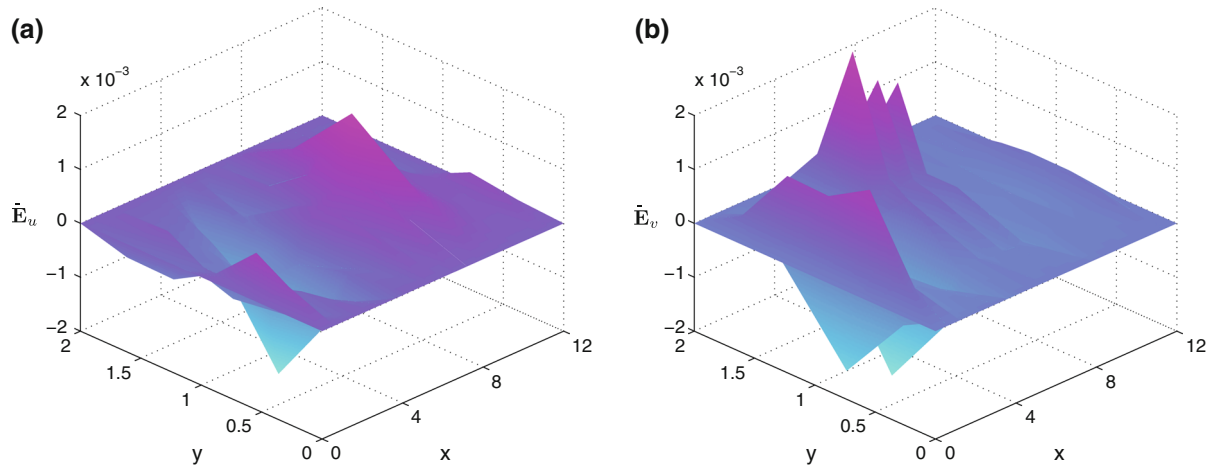

Fig. 4 Error of FEM solution with 132 nodes and 212 elements. **a** Error distribution for horizontal displacement $\bar{\mathbf{E}}_u$. **b** Error distribution for vertical displacement $\bar{\mathbf{E}}_v$

Other boundary conditions frequently used for the Timoshenko beam problem are as follows:

A. $u = v = 0$ at $x = 0$ and $P' = 5$ per unit length at $x = L$ (Figs. 2 and 3).
B. u and v given by Eqs. (12a) and (12b) at $x = 0$ and $P' = -(6\,P)/D^3)\,(y^2 - D\,y)$ at $x = L$.

Only boundary conditions B produce exactly the solution in Eqs. (12a) and (12b). In the rest of the paper we will use Dirichlet boundary conditions given by (12a) and (12b) in all boundaries of the beam $x = 0,\ x = L,\ y = 0,\ y = D$, and in this way we will be able to use the exact solution for displacements (12a) and (12b) and stresses (13a)–(13c) when computing numerical errors with the proposed RBF methods.

3.1.1 FEM solution

For comparison purposes, we will first compute the solution using FEMs on a mesh of 132 nodes and 212 elements. We denote the solution in horizontal and vertical displacements as u_{FEM} and v_{FEM} and the corresponding errors as

$$\bar{\mathbf{E}}_u = u_{\text{FEM}} - u_e \quad \text{and} \quad \bar{\mathbf{E}}_v = v_{\text{FEM}} - v_e.$$

Figure 4 shows the error in the horizontal and vertical displacements ($\bar{\mathbf{E}}_u$ and $\bar{\mathbf{E}}_v$) resulting from solving the Timoshenko beam problem with Dirichlet boundary conditions using a FEM. The infinity norm of the error in u is $||\bar{\mathbf{E}}_u||_\infty = 2.544 \times 10^{-3}$ and the Euclidean norm is $||\bar{\mathbf{E}}_u||_2 = 5.147 \times 10^{-3}$. The corresponding values for the vertical displacements are $||\bar{\mathbf{E}}_u||_\infty = 2.881 \times 10^{-3}$ and $||\bar{\mathbf{E}}_u||_2 = 6.931 \times 10^{-3}$.

3.1.2 Global RBF solution

We can compute the solution with the global RBF method using as RBF centers exactly the same nodes of the FEM mesh. For convenience we will use the same value of the shape parameter both for horizontal, u, and vertical, v, displacements ($c_u = c_v = c$). We will use the following measure of error:

$$\mathbf{E}_u = u - u_e \quad \text{and} \quad \mathbf{E}_v = v - v_e,$$

so that

$$E = ||\mathbf{E}_u||_\infty + ||\mathbf{E}_v||_\infty. \tag{14}$$

Figure 5 shows the sum of the infinity norms of the errors in horizontal and vertical displacements of the global RBF solution as a function of the shape parameter c. The solid line shows the results obtained with the same

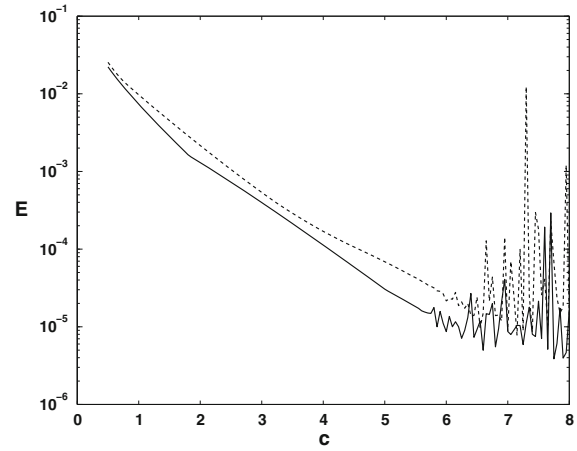

Fig. 5 Error of global RBF solution, E, as a function of the shape parameter c. *Solid*: $N = 132$ nonequispaced RBF centers; *dashed*: $N = 19 \times 7 = 133$ equispaced nodes

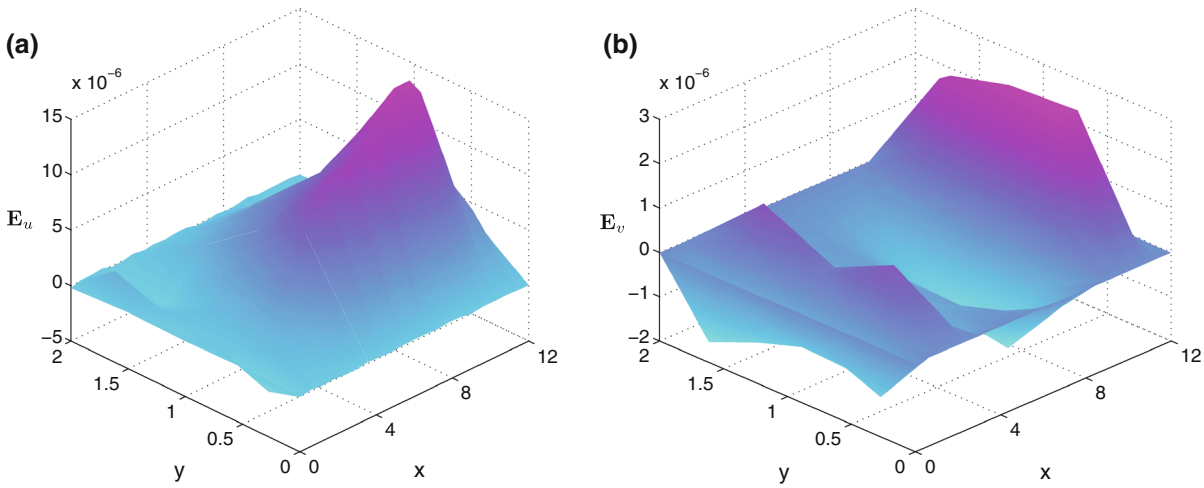

Fig. 6 Error of global RBF solution for $c_u = c_v = 6$ and $N = 132$ RBF centers. **a** Error distribution for horizontal displacement $\mathbf{E}_u$. **b** Error distribution for vertical displacement $\mathbf{E}_v$

$N = 132$ unequally spaced nodes used in the FEM solution, and the dashed line shows the results obtained on an equally spaced mesh of $N = 19 \times 7 = 133$ equally spaced nodes. Notice that both curves exhibit exponential convergence of the error with increasing c. Also notice that for shape parameter values larger than approximately 6 the resulting matrix becomes ill-conditioned, and convergence is no longer a smooth function. It should be pointed out that for the same number of nodes the global RBF solution is significantly more accurate than the FEM solution. For instance, the results for a value of the shape parameter $c = 6$ are shown in Fig. 6. Notice that there is approximately three-order-of-magnitude increase in accuracy if one compares Fig. 6 to the error of the FEM solution shown in Fig. 4. In fact, the infinity norm of the error in u is $||\mathbf{E}_u||_\infty = 1.868 \times 10^{-5}$ and the Euclidean norm is $||\mathbf{E}_u||_2 = 6.348 \times 10^{-5}$. The infinity norm of the error in v is $||\mathbf{E}_v||_\infty = 2.872 \times 10^{-6}$ and the Euclidean norm is $||\mathbf{E}_v||_2 = 1.027 \times 10^{-5}$. However, it should be pointed out that the linear system that must be solved in order to compute the numerical solution with the global RBF method is dense, whereas in the case of the FEM it is sparse. Thus, for the same number of nodes, the computational cost of the global RBF method is higher than the computational cost of the FEM.

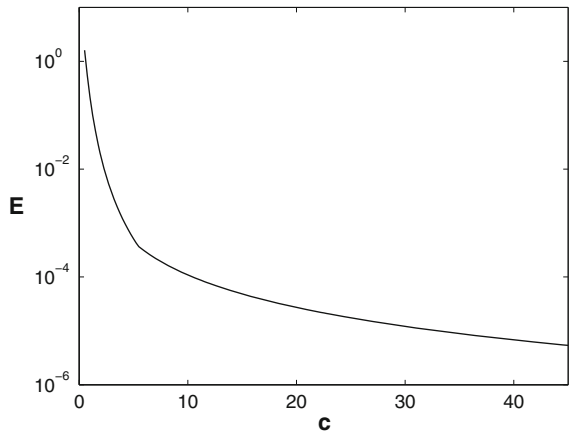

Fig. 7 Error of RBF local solution, E, as a function of c. Equispaced grid of $N = 19 \times 7 = 133$ nodes

3.1.3 Local RBF solution

To compute the solution with the RBF local method we have to select a set of N nodes and for each node a stencil of n surrounding nodes. For convenience we will use a grid of equispaced nodes and, for each node (x_i, y_i) a stencil of three adjacent nodes (x_i, y_i), $(x_i - \Delta x, y_i)$, $(x_i + \Delta x, y_i)$ in the horizontal direction to approximate ∂_{xx}, three nodes in the vertical direction (x_i, y_i), $(x_i, y_i - \Delta y)$, $(x_i, y_i + \Delta y)$ to approximate ∂_{yy}, and five nodes (x_i, y_i), $(x_i - \Delta x, y_i - \Delta y)$, $(x_i + \Delta x, y_i - \Delta y)$, $(x_i + \Delta x, y_i + \Delta y)$, $(x_i - \Delta x, y_i + \Delta y)$ to approximate ∂_{xy}.

Figure 7 shows the error as a function of the shape parameter for a grid of $N = 19 \times 7 = 133$ equispaced nodes. In this case we have taken the shape parameters for all the derivatives appearing in (1) as being equal ($c_{uxx} = c_{uyy} = c_{uxy} = c_{vxx} = c_{vyy} = c_{vxy} = c$). Notice that the exponential convergence of the global method has been lost and that the error E of the local method decreases as c^{-2}. This behavior should be expected according to the formulas for the error of the RBF local method derived in [28]. In fact, the formula for the error in approximating the second derivative with respect to x using three equispaced nodes (see Eq. 14 in [28]) is

$$\epsilon_3(u_{xx}) = \frac{(\Delta x)^2}{12}\frac{\partial^4 u}{\partial x^4} + \frac{(\Delta x)^4}{c^2}\frac{\partial^2 u}{\partial x^2} - \frac{3\,(\Delta x)^2}{4\,c^4}u + \cdots .$$

Similarly,

$$\epsilon_3(u_{yy}) = \frac{(\Delta y)^2}{12}\frac{\partial^4 u}{\partial y^4} + \frac{(\Delta y)^4}{c^2}\frac{\partial^2 u}{\partial y^2} - \frac{3(\Delta y)^2}{4c^4}u + \cdots .$$

Because the solutions for u and v of the Timoshenko beam problem [Eqs. (12a) and (12b)] are polynomials of third degree, u_{xxxx}, u_{yyyy}, v_{xxxx}, and v_{yyyy} are zero. Thus, the errors in approximating the second derivatives of u and v approach zero as c approaches infinity. In fact, it is well known that RBF–FD formulas approach standard FDs when $c \to \infty$. Therefore, for this particular problem standard FDs yield the exact solution of the problem, and the RBF–FD error approaches zero as $c \to \infty$ ($E \approx O(c^{-2})$).

3.2 Plate with a hole

Let us consider the problem of an infinite plate with a hole of radius a loaded by a traction σ_0 at infinity in the x direction [26, p. 76]. This problem has been used often as a test case to assess the accuracy of different meshless methods [5,7,29]. In Cartesian coordinates the exact solution can be written as

$$u_e = \frac{\sigma_0 a}{8G}\left[\frac{x}{a}(\kappa+1) + 2a(1+\kappa)\frac{x}{x^2+y^2} + 2a\frac{x^3-3xy^2}{(x^2+y^2)^2}\left(1 - \frac{a^2}{x^2+y^2}\right)\right], \tag{15a}$$

$$v_e = \frac{\sigma_0 a}{8G}\left[\frac{y}{a}(\kappa-3) + 2a(1-\kappa)\frac{y}{x^2+y^2} + 2a\frac{3yx^2-y^3}{(x^2+y^2)^2}\left(1 - \frac{a^2}{x^2+y^2}\right)\right], \tag{15b}$$

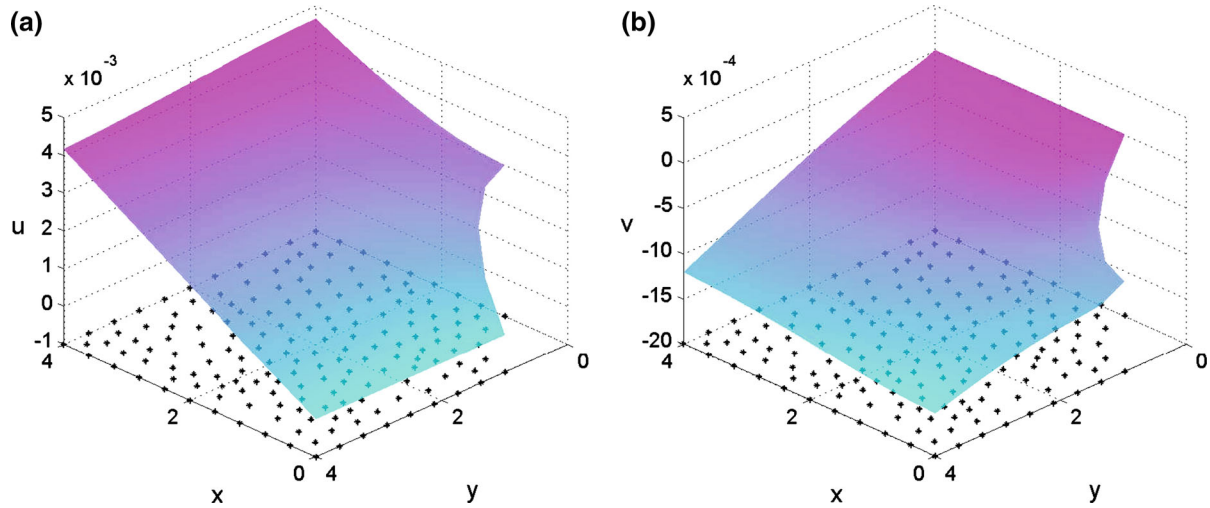

Fig. 8 RBF global solution for the case $N = 174$, $c_u = c_v = 2$. **a** Horizontal displacement u. **b** Vertical displacement v

where

$$G = \frac{E}{2\,(1+\nu)} \quad \text{and} \quad \kappa = \frac{3-\nu}{1+\nu}.$$

The corresponding stresses are

$$\sigma_{xx} = \sigma_0 \left[1 - \frac{3}{2}\frac{a^2(x^2-y^2)}{(x^2+y^2)^2} - \frac{a^2}{(x^2+y^2)^3}(x^4+y^4-6x^2y^2)\left(1-\frac{3}{2}\frac{a^2}{x^2+y^2}\right)\right],$$

$$\sigma_{yy} = \sigma_0 \left[-\frac{1}{2}\frac{a^2(x^2-y^2)}{(x^2+y^2)^2} + \frac{a^2}{(x^2+y^2)^3}(x^4+y^4-6x^2y^2)\left(1+\frac{3}{2}\frac{a^2}{x^2+y^2}\right)\right],$$

$$\tau_{xy} = -\sigma_0 \left[\frac{a^2xy}{(x^2+y^2)^2} + 4a^2xy\frac{x^2-y^2}{(x^2+y^2)^3}\left(1+\frac{3}{2}\frac{a^2}{x^2+y^2}\right)\right].$$

3.2.1 Global RBF solution

We solve the problem with $\sigma_0 = 1$, $E = 1{,}000$, $L_x = 4$, $L_y = 4$, $a = 1$, $\nu = 0.3$ and Dirichlet boundary conditions. We use a set of 174 RBF centers that coincide with the nodes of a triangular mesh used to compute the solution with the FEM. Figure 8 shows the RBF numerical solution for horizontal (Fig. 8a) and vertical (Fig. 8b) displacements using $c_u = c_v = 2$. Also shown are the nodes used as RBF centers.

Figure 9 shows the error (14) of the global RBF solution as a function of the shape parameter ($c_u = c_v = c$) for two different sets of RBF centers. In the case $N = 633$, the error exhibits exponential convergence until a value of $c \approx 1.6$ is reached for which the matrix becomes ill-conditioned and roundoff errors deteriorate the accuracy of the solution. The exponential convergence can also be observed in the case $N = 174$. However, in this case, ill-conditioning occurs for values of the shape parameter larger than those shown in the figure.

It is also possible to use a minimization routine (we used the `fminsearch` function in MATLAB) to find values of c_u and c_v that minimize the error. For the coarser grid ($N = 174$) the error E is at a minimum for $c_u = 2.8803$, $c_v = 1.5480$ ($||\mathbf{E}_u||_\infty = 1.72 \times 10^{-5}$, $||\mathbf{E}_v||_\infty = 1.26 \times 10^{-5}$). For the finer grid ($N = 653$) the error is at a minimum for $c_u = 1.6364$, $c_v = 1.4401$ ($||\mathbf{E}_u||_\infty = 1.21 \times 10^{-6}$, $||\mathbf{E}_v||_\infty = 9.10 \times 10^{-7}$).

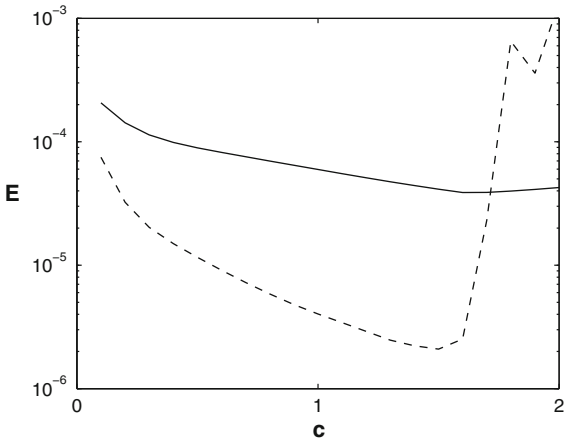

Fig. 9 Error (14) as a function of shape parameter c. *Solid line*: $N = 174$ RBF centers; *dashed line*: $N = 653$ RBF centers

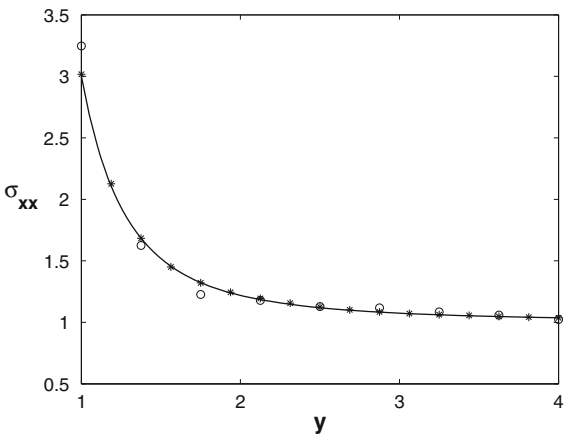

Fig. 10 Stress σ_{xx} as a function of y at left boundary ($x = 0$) obtained using global RBF method. *Solid line*: exact solution. *Open circle*: 174 RBF centers. *Asterisk*: 653 RBF centers

Figure 10 shows the stress σ_{xx} along the left boundary ($x = 0$) for two sets of RBF centers. For $N = 174$ RBF centers there are significant discrepancies with the analytical solution, especially in the vicinity of the hole ($y \approx 1$). For $N = 653$ RBF centers the RBF solution is very accurate for all values of y.

3.2.2 Local RBF solution

The solution of the plate-with-a-hole problem [Eqs. (15a) and (15b)] is no longer a polynomial, and therefore its solution with standard FDs is no longer exact. We will use RBF–FD formulas to compute the solution both on an equispaced grid and on a nonequispaced grid.

Equispaced nodes For simplicity, we will start by using an equispaced grid made up of nodes that are in the boundary or in the interior of the plate. We denote by N the number of such nodes in the interior or in the boundary of the plate. To compute second derivatives, we use three node stencils, (x_i, y_i), $(x_i - \Delta x, y_i)$, $(x_i + \Delta x, y_i)$, to approximate u_{xx} and v_{xx}, and we use (x_i, y_i), $(x_i, y_i - \Delta y)$, $(x_i, y_i + \Delta y)$ to approximate u_{yy} and v_{yy}. To compute crossed derivatives, we use five node stencils, (x_i, y_i), $(x_i - \Delta x, y_i - \Delta y)$, $(x_i - \Delta x, y_i + \Delta y)$, $(x_i + \Delta x, y_i - \Delta y)$ $(x_i + \Delta x, y_i + \Delta y)$, to approximate u_{xy} and v_{xy}. We consider as interior nodes those whose six neighbors belong to the set of nodes and as boundary nodes those that have at least one neighbor that does not belong to the set of nodes. At interior nodes we apply the RBF–FD formulation, and at boundary nodes we apply Dirichlet boundary conditions given by (15a) and (15b).

Figure 11 shows the error as a function of the shape parameter for three different grids: 21×21 ($N = 419$), 31×31 ($N = 909$), and 41×41 ($N = 1{,}595$). In all cases the error increases for very small values of c, then decreases exponentially with increasing c, and approaches a constant for larger values of c. This constant corresponds to the error resulting from standard FD.

In a recent paper [28] we showed that frequently there is an optimal value of the shape parameter such that the local approximation error resulting from RBF–FD formulas is at a minimum. We also showed [23,24] that using at each node the corresponding optimal shape parameter may lead to very significant improvements in accuracy. In what follows, we will apply this technique to compute accurate solutions of the plate-with-a-hole problem.

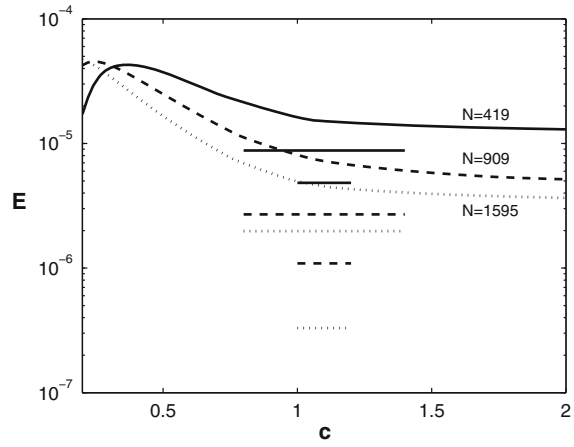

Fig. 11 Error (14) as a function of shape parameter c with local method. *Solid line*: 21×21 ($N = 419$) nodes; *dashed line*: 31×31 ($N = 909$); *dotted line*: 41×41 ($N = 1{,}595$); *long horizontal lines*: error (14) using the optimal, node-dependent shape parameter: *short horizontal lines*: Error (14) using generalized multiquadrics

For simplicity of the resulting formulas, we add a constant term to the RBF interpolation space [30], so that Eq. (8) is replaced by

$$w(\mathbf{x}) = \sum_{i=1}^{n} \lambda_i \phi(r_i(\mathbf{x}), c) + \beta.$$

In [28] we derived an approximate equation for the local error resulting from RBF–FD formulas for second derivatives using three equispaced nodes (see Eq. 14 in [28]]. Adding the constant term, the error formula for u_{xx} is modified to

$$\hat{\epsilon}_3(x, y) \approx \frac{(\Delta x)^2}{12} \frac{\partial^4 u}{\partial x^4} + \frac{5}{4} \frac{(\Delta x)^2}{c^2} \frac{\partial^2 u}{\partial x^2}. \tag{16}$$

Therefore, the error is zero for

$$c^* = \sqrt{-\frac{15 u_{xx}}{u_{xxxx}}}.$$

This is the optimal value that we use at each node to approximate second derivatives. Notice that if the expression inside the square root is not positive, then there is no real value of c that makes the local approximation error null.

Analogously, for the cross derivative, the local approximation error using an equispaced five node stencil is

$$\hat{\epsilon}_5 \approx \frac{1}{6} \left(\frac{\partial^4 u}{\partial x^3 \partial y} (\Delta x)^2 + \frac{\partial^4 u}{\partial x \partial y^3} (\Delta y)^2 \right) + \frac{3}{2c^2} \frac{\partial^2 u}{\partial x \partial y} \left((\Delta x)^2 + (\Delta y)^2 \right). \tag{17}$$

In the case $\Delta x = \Delta y$, the optimal shape parameter ($\hat{\epsilon}_5 \approx 0$) is

$$c^* = \sqrt{-\frac{18 u_{xy}}{u_{xxxy} + u_{xyyy}}}. \tag{18}$$

Applying these formulas with the derivatives appearing in them computed from the exact solution (15a), (15b) at each node of the grid, we can compute the optimal shape parameter to approximate each of the derivatives of u and v appearing in (1). In real applications, when the exact solution is not known, the derivatives appearing in (18) are estimated using the procedure described in [23,24].

Figure 12 shows the nodes for which an optimal shape parameter exists for u_{xx} (Fig. 12a) and u_{yy}. These results correspond to the grid of 31×31 ($N = 909$) nodes. Notice that there is a large number of nodes for which no optimal shape parameter exists. In those nodes we use standard FD. Similar results apply to the optimal shape parameter corresponding to v_{xx}, v_{yy}, u_{xy} and v_{xy}.

Figure 13 shows the spatial distribution of the optimal shape parameter for the cross derivative of the vertical displacement, v_{xy}. The results correspond to a grid of 41×41 ($N = 1{,}595$) nodes. At nodes where no c^* exists,

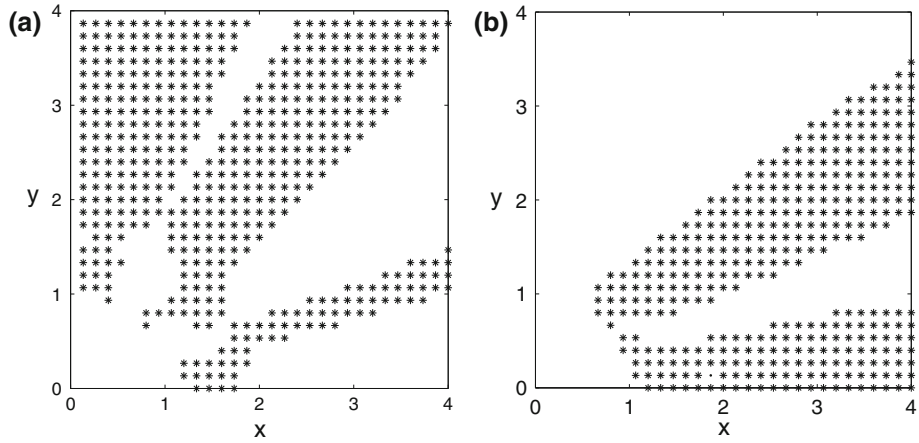

Fig. 12 **a** Nodes where optimal c to approximate u_{xx} exists. **b** Nodes where optimal c to approximate u_{yy} exists

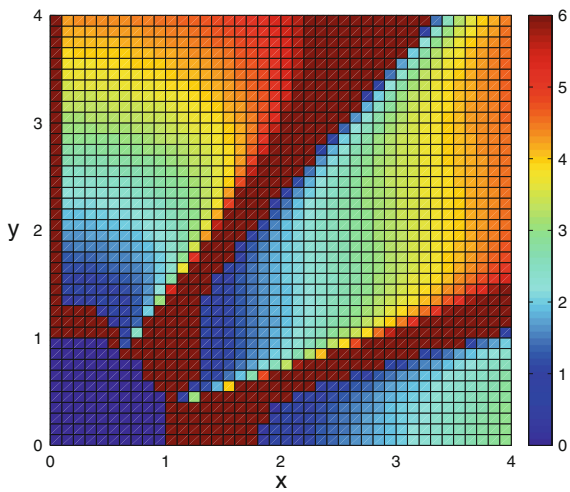

Fig. 13 Distribution of optimal shape parameter corresponding to v_{xy}. $N = 1{,}595$

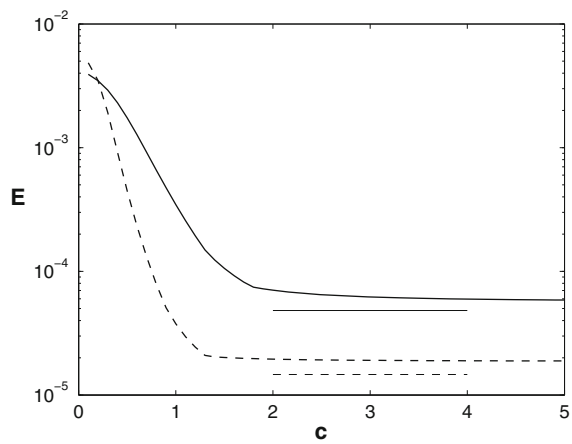

Fig. 14 Error (14) as a function of theshape parameter c with the local method. *Solid line*: $n = 174$ nodes; *dashed line*: $n = 653$ nodes; *thin lines*: different shape parameters for each derivative

we have assigned a value $c^* = 6$. For such a large value of c the RBF–FD formulas are equivalent to standard FDs. Notice that the optimal shape parameter varies smoothly and its minimum value is 0.1810.

The error measures (14) resulting from applying the RBF–FD method with the optimal shape parameter at each node are shown as long horizontal lines in Fig. 11 for the three grids analyzed. Notice that there are significant accuracy improvements with respect to the results obtained with a constant shape parameter for all nodes and all derivatives.

In Ref. [24] it was observed that the increase in accuracy resulting from the use of an optimal shape parameter at each node strongly depended on the percentage of nodes for which the optimal shape parameter existed. Hence, we proposed [24] the use of generalized multiquadrics to ensure that the RBF–FD local approximation error was zero to leading order at all nodes. In fact, the generalized multiquadric

$$\phi_k((||\mathbf{x} - \mathbf{x}_k||, c, \beta) = \left[(x - x_k)^2 + (y - y_k)^2 + c^2\right]^{\beta/2} \tag{19}$$

has an additional parameter β (node-dependent) that can be chosen such that an optimal value of the shape parameter exists at every node. Implementing this procedure to the solution of problem (15a)–(15b) results in the errors shown with a short horizontal line in Fig. 11. As expected, this procedure leads to significant improvements in accuracy. For instance, in the case of $N = 1{,}595$ the error (14) with FD is 3.94×10^{-6}, the error with the optimal shape parameter using standard multiquadrics is 1.97×10^{-6}, and the error with the optimal shape parameter using generalized multiquadrics is 4.52×10^{-7}. Similar improvements are observed for $N = 419$ and 909.

Nonequispaced nodes We can also solve the problem with the local method using nonequispaced nodes. For each node, we select a stencil made up of the five nearest neighbors ($n = 6$ stencils), and for each differential operator and each node we compute the coefficients α_{ji} of the stencil by solving the 6×6 linear system defined in Eq. (11). Figure 14 shows the error (14) as a function of the shape parameter c for the grid of $N = 174$ nodes shown in Fig. 8 (solid line). Also shown is the error as a function of c for a grid of $N = 653$ nodes (dashed line) obtained by refining the initial mesh. Notice that the error dependence with c of the nonequispaced case is similar to that observed for the equispaced case (Fig. 11): the error decreases with increasing c and approaches a constant for large values of c. However, the errors for the nonequispaced case are significantly smaller than those of the equispaced case. The reason for this is that the nodes in the vicinity of the inner circle, where the errors are larger, are better distributed in the nonequispaced case than in the case of a regular equispaced grid. Also shown (thin lines) are the errors resulting from using a different shape parameter for each derivative. In the case $N = 175$, the optimal shape parameters for u_{xx}, u_{yy}, v_{xx}, v_{yy}, u_{xy}, and v_{xy} are 14.2323, 1.7069, 1.4298, 1.9374, 5.3884, and 13.0723, respectively. In the case $N = 653$, the corresponding values of the shape parameters are 8.6361, 1.5943, 5.0336, 1.2891, 9.9104, and 8.1346, respectively. These values are obtained using the `fminsearch` function in MATLAB to minimize the error. Notice the slight improvement in accuracy.

4 Conclusions

In this paper we described the global and local versions of the RBF method and analyze their applicability to the solution of two standard elastostatic problems: the Timoshenko beam problem and the problem of an infinite plate with a circular hole. The objective of our work was to show how accuracy could be significantly increased by efficiently tuning the values of shape parameters. We used multiquadrics as RBFs both for the global and local methods, and we described how to select an optimal value of the shape parameter to minimize approximation errors. For the local method, the selection of the optimal shape parameter was based on analytical approximations to the local error that we derived recently [28] using either the same shape parameter at all nodes [23] or a node-dependent shape parameter [24]. We used both equispaced and nonequispaced nodes, and we showed that significant gains in accuracy resulted from a proper selection of the shape parameter.

Acknowledgments This work was supported by Spanish MICINN Grants FIS2011-28838 and CSD2010-00011 and by Madrid Autonomous Region Grant S2009-1597. M.K. acknowledges Fundación Caja Madrid for its financial support.

References

1. Fasshauer GE (2007) Meshfree approximation methods with MATLAB. World Scientific, Singapore
2. Kansa EJ (1990) Multiquadrics, a scattered data approximation scheme with applications to computational fluid dynamics I. Surface approximations and partial derivatives estimates. Comput Math Appl 19:127–145
3. Kansa EJ (1990) Multiquadrics, a scattered data approximation scheme with applications to computational fluid dynamics II. Solutions to parabolic, hyperbolic and elliptic partial differential equations. Comput Math Appl 19:147–161
4. Shu C, Ding H, Yeo KS (2003) Local radial basis function-based differential quadrature method and its application to solve two-dimensional incompressible Navier–Stokes equations. Comput Methods Appl Mech Eng 192:941–954
5. Tolstykh AI, Shirobokov AI (2003) On using radial basis functions in a "finite difference mode" with applications to elasticity problems. Comput Mech 33b:68–79
6. Wright GB (2003) Radial basis function interpolation: numerical and analytical developments. Ph.D. thesis, University of Colorado, Boulder

7. Zhang X, Song KZ, Lu MW, Liu X (2000) Meshless methods based on collocation with radial basis functions. Comput Mech 26:333–343
8. Wendland H (1995) Piecewise polynomial positive definite and compactly supported radial basis functions of minimal degree. Adv Comput Math 4:389–396
9. Liu GR, Gu YT (2001) A local radial point interpolation method (LRPIM) for free vibration analyses of 2-d solids. J Sound Vib 246:29–46
10. Wang JG, Liu GR (2002) A point interpolation meshless method based on radial basis functions. Int J Numer Methods Eng 54:1623–1648
11. Ferreira AJM (2003) A formulation of the multiquadric radial basis function method for the analysis of laminated composite plates. Compos Struct 59:385–392
12. Ferreira AJM (2003) Thick composite beam analysis using a global meshless approximation based on radial basis functions. Mech Adv Mater Struct 10:271–284
13. Ferreira AJM, Roque CMC, Martins PALS (2004) Radial basis function and higher-order shear deformation theories in the analysis of laminated composite beams and plates. Compos Struct 66:287–293
14. Ferreira AJM, Roque CMC, Jorge RMN, Kansa EJ (2005) Static deformations and vibrations analysis of composite and sandwich plates using a layerwise theory and multiquadrics discretizations. Compos Struct 29:1104–1114
15. Ferreira AJM, Roque CMC, Fasshauer GE, Jorge RMN, Batra RC (2007) Analysis of functionally graded plates by a robust meshless method. Mech Adv Mater Struct 14:577–587
16. Leitao VMA (2001) A meshless method for Kirchhoff plate bending problems. Int J Numer Methods Eng 52:1107–1130
17. Roque CMC, Ferreira AJM, Jorge RMN (2007) A radial basis function approach for the free vibration analysis of functionally graded plates using a refined theory. J Sound Vib 300:1048–1070
18. Ferreira AJM, Fasshauer GE (2006) Computation of natural frequencies of shear deformable beams and plates by an RBF-pseudospectral method. Comput Methods Appl Mech Eng 196:134–146
19. Ferreira AJM, Fasshauer GE, Batra RC, Dias Rodrigues J (2008) Static deformations and vibrations analysis of composite and sandwich plates using a layerwise theory nd RBF-PS discretizations with optimal shape parameter. Compos Struct 86:328–343
20. Roque CMC, Cunha D, Shu C, Ferreira AJM (2011) A local radial basis functions—finite differences technique for the analysis of composite plates. Eng Anal Boundary Elements 35:363–374
21. Liew KM, Chen XL, Reddy JN (2004) Mesh-free radial basis function method for buckling analysis of non-uniformly loaded arbitrarily shaped shear deformable plates. Comput Methods Appl Mech Eng 193:205–224
22. Liu GR, Zhang GY, Gu YT (2005) A meshfree radial point interpolation method (RPIM) for three dimensional solids. Comput Mech 36:421–430
23. Bayona V, Moscoso M, Kindelan M (2011) Optimal constant shape parameter for multiquadric based RBF-FD method. J Comput Phys 230:7384–7399
24. Bayona V, Moscoso M, Kindelan M (2012) Optimal variable shape parameter for multiquadric based RBF-FD method. J Comput Phys 231:2466–2481
25. Hardy RL (1971) Multiquadric equations of topography and other irregular surfaces. J Geophys Res 176:1905–1915
26. Timoshenko SP, Goodier JN (1951) Theory of elasticity. McGraw-Hill, New York
27. Augarde CE, Deeks AJ (2008) The use of Timoshenko's exact solution for a cantilever beam in adaptive analysis. Finite Elements Anal Des 44:595–601
28. Bayona V, Moscoso M, Carretero M, Kindelan M (2010) RBF-FD formulas and convergence properties. J Comput Phys 229:8281–8295
29. Hsu-Kuang C (2002) Solution of linear elastostatic and elastodynamic plane problems by the meshless local Petrov–Galerkin method. Ph.D. dissertation, Virginia Polytechnic Institute and State University, Blacksburg, VA
30. Wright GB, Fornberg B (2006) Scattered node compact finite difference-type formulas generated from radial basis functions. J Comput Phys 212:99–123